Geophysical Research Letters

RESEARCH LETTER
10.1029/2023GL104667

Impacts of Volcanic Emissions on the Global Biogeochemical Mercury Cycle: Insights From Satellite Observations and Chemical Transport Modeling

Benjamin M. Geyman[1], Colin P. Thackray[1], Daniel J. Jacob[1], and Elsie M. Sunderland[1,2]

[1]Harvard John A. Paulson School of Engineering and Applied Sciences, Cambridge, MA, USA, [2]Department of Environmental Health, Harvard School of Public Health, Boston, MA, USA

Key Points:

- Volcanic mercury emissions of 232 Mg a^{-1} (IQR: 170–336 Mg a^{-1}) are estimated by indexing to sulfur dioxide from satellite remote sensing
- Over 90% of volcanic mercury emissions occur in the tropics and mid-latitude Northern Hemisphere
- Volcanic emissions support a pre-anthropogenic atmospheric mercury reservoir of approximately 580 Mg (7-fold lower than in 2015)

Supporting Information:

Supporting Information may be found in the online version of this article.

Correspondence to:

B. M. Geyman,
bgeyman@fas.harvard.edu

Citation:

Geyman, B. M., Thackray, C. P., Jacob, D. J., & Sunderland, E. M. (2023). Impacts of volcanic emissions on the global biogeochemical mercury cycle: Insights from satellite observations and chemical transport modeling. *Geophysical Research Letters*, *50*, e2023GL104667. https://doi.org/10.1029/2023GL104667

Received 3 JUN 2023
Accepted 11 SEP 2023

Author Contributions:

Conceptualization: Benjamin M. Geyman, Elsie M. Sunderland
Data curation: Benjamin M. Geyman
Formal analysis: Benjamin M. Geyman
Funding acquisition: Elsie M. Sunderland
Methodology: Benjamin M. Geyman, Colin P. Thackray, Elsie M. Sunderland
Project Administration: Elsie M. Sunderland
Resources: Elsie M. Sunderland
Supervision: Daniel J. Jacob, Elsie M. Sunderland

Abstract Volcanism is the largest natural source of mercury (Hg) to the biosphere. However, past Hg emission estimates have varied by three orders of magnitude. Here, we present an updated central estimate and interquartile range (232 Mg a^{-1}; IQR: 170–336 Mg a^{-1}) for modern volcanic Hg emissions based on advances in satellite remote sensing of sulfur dioxide (SO_2) and an improved method for considering uncertainty in Hg:SO_2 emissions ratios. Atmospheric modeling shows the influence of volcanic Hg on surface atmospheric concentrations in the extratropical Northern Hemisphere is 1.8 times higher than in the Southern Hemisphere. Spatiotemporal variability in volcanic Hg emissions may obscure atmospheric trends forced by anthropogenic emissions at some locations. This should be considered when selecting monitoring sites to inform global regulatory actions. Volcanic emission estimates from this work suggest the pre-anthropogenic global atmospheric Hg reservoir was 580 Mg, 7-fold lower than in 2015 (4,000 Mg).

Plain Language Summary Volcanism is widely recognized as the most important natural source of mercury (Hg) globally, but existing emissions estimates contain substantial uncertainty. This study combines satellite observations of sulfur dioxide (SO_2) in volcanic plumes and measured Hg:SO_2 ratios to quantify the magnitude and spatiotemporal variability of global volcanic Hg emissions. Using a global model, we show that the spatial pattern of volcanic releases and atmospheric dynamics result in greater concentrations of volcanic Hg in the mid-latitude Northern Hemisphere compared to the mid-latitude Southern Hemisphere. Modeling results suggest that variability in volcanic Hg emissions at some locations may obscure trends in atmospheric Hg concentrations driven by human emissions. The influence of volcanic Hg emissions should therefore be considered during selection of global monitoring sites used to track the progress of regulatory actions designed to mitigate Hg pollution. Volcanic release estimates from this work suggest the natural atmospheric Hg reservoir was ~7 times smaller than in 2015, reinforcing that humans have profoundly disrupted the global biogeochemical Hg cycle.

1. Introduction

Mercury (Hg) is a priority pollutant in the biosphere due to its toxicity and strong biomagnification in food webs (Obrist et al., 2018). Despite decades of research, there is still considerable debate about the amount of natural Hg in the environment (Edwards et al., 2021; Pyle & Mather, 2003). Volcanoes are the main natural Hg source to the biosphere, and past estimates of annual emissions vary by three orders of magnitude (<1 to 1,000 Mg a^{-1}) (Ferrara et al., 2000; Nriagu, 1989; Varekamp & Buseck, 1981). Little is known about spatial and temporal variability in Hg releases from volcanic Hg sources, which is important for interpreting changes in atmospheric Hg concentrations and deposition at specific locations. Here we present refined estimates of volcanic Hg releases and their fate in the global environment based on advances in satellite monitoring of sulfur dioxide (SO_2) and global modeling.

Volcanic Hg emissions are typically estimated by indexing Hg releases to sulfur dioxide (SO_2) fluxes. Differences in magma composition, gas chemistry, and emission temperatures can lead to spatial (Bagnato et al., 2015) and temporal variability (Witt et al., 2008a, 2008b) in Hg:SO_2 ratios (Aiuppa et al., 2007; Bagnato et al., 2007). In volcanic plumes, SO_2 is enriched relative to the background atmosphere and can be measured by remote sensing because it absorbs ultraviolet light. Global satellite monitoring provides high-resolution estimates of small (~8 kt SO_2 a^{-1}) and diffuse volcanic sources (Carn et al., 2016, 2017; Fioletov et al., 2023). Global estimates

Writing – original draft: Benjamin M. Geyman
Writing – review & editing: Benjamin M. Geyman, Colin P. Thackray, Daniel J. Jacob, Elsie M. Sunderland

of volcanic SO_2 emissions have increased from 13 to >20 Tg a^{-1} due to improvements in satellite sensors and extended spatial/temporal coverage (Andres & Kasgnoc, 1998; Carn et al., 2016, 2017; Fioletov et al., 2023).

Volcanic plume injection altitude and Hg speciation both affect the atmospheric lifetime of emissions and spatial patterns of subsequent deposition. Some explosive eruptions inject Hg into the upper troposphere and lower stratosphere, which extends the lifetime of Hg prior to deposition and increases long-range transport (Gratz et al., 2015). The long half-life of elemental Hg (Hg^0) in the troposphere allows hemispheric to global transport after release, but other forms (Hg^{II} species, including particle-bound) are highly water soluble and deposit rapidly (Horowitz et al., 2017). Rapid redox reactions in volcanic plumes cause Hg:SO_2 ratios to change during plume dispersal (Aiuppa et al., 2007; Bagnato et al., 2011; Von Glasow, 2010; Zambardi et al., 2009). Halogens known to oxidize Hg^0 are co-emitted from volcanoes, increasing Hg^{II} in plumes and decreasing atmospheric Hg lifetime (Von Glasow, 2010; Zambardi et al., 2009). Some prior measurements suggest that >90% of volcanic Hg emissions are present as Hg^0 immediately after degassing (Bagnato et al., 2007, 2011; Witt et al., 2008a, 2008b). However, available measurements from sites in Italy (Dedeurwaerder et al., 1982; Zambardi et al., 2009) and model calculations (Von Glasow, 2010) suggest rapid oxidation of Hg^0 occurs as the plume ages, sustaining up to 60% of total Hg as Hg^{II}. While oxidant concentrations and volcanic plume altitude are known to be important for Hg deposition patterns, neither has been evaluated in past work.

The main objectives of this work are to: (a) develop improved Hg emissions estimates from volcanism and (b) simultaneously consider the influence of both atmospheric dynamics and chemistry on the spatial patterns of Hg deposition attributable to volcanic sources. We use timeseries data of satellite-derived volcanic SO_2 emissions (Carn, 2022; Edwards et al., 2021; Fioletov et al., 2023) and measured variability in volcanic plume Hg:SO_2 ratios to characterize spatial and temporal variability in global Hg releases from volcanism. We simulate volcanic Hg deposition from 2005 through 2021 by forcing the GEOS-Chem global 3-D atmospheric chemical transport model (Shah et al., 2021) with refined emissions estimates from volcanism. These results provide insights into the contributions of volcanic Hg to contemporary atmospheric observations and the atmospheric lifetimes of Hg emitted from different categories of volcanism. Finally, we use a geochemical box model to reconstruct the natural Hg budget prior to human influence based on the updated volcanic Hg releases estimated in this study.

2. Data and Methods

2.1. Spatial and Temporal Hg Emissions From Global Volcanism

We estimated emissions for three categories of volcanism: *passive degassing* (gaseous emission with no coincident eruption of magma), *effusive eruptions* (outpouring of lava onto the ground), and *explosive eruptions* (expulsion of volcanic ash and gases into the atmosphere following depressurization at the vent). We used the global catalog of large anthropogenic and volcanic SO_2 sources to estimate passive degassing fluxes from 2005 to 2021 (Fioletov et al., 2023). These data were generated using retrievals from multiple satellite spectrometers (OMPS, OMI, TROPOMI) (Fioletov et al., 2023). Uncertainties in SO_2 emissions from passive degassing were assumed to follow a Gaussian distribution and varied from 4% to 81% among individual sources depending on source magnitude, satellite overpass frequency, vent elevation, and albedo (Fioletov et al., 2023).

Eruptive SO_2 emissions data were from the Multi-Satellite Volcanic Sulfur Dioxide Database (v4), which cataloged explosive and effusive eruptions that occurred between 1978 and 2022 (Carn, 2022). For effusive and explosive eruptions, we assumed uniformly distributed SO_2 emission uncertainties based on past work of ±50% for smaller eruptions with a volcanic explosivity index of <4 and ±20% for larger eruptions (VEI ≥ 4) (Ge et al., 2016). The emission data set included 194 independent volcanic sources. The Supporting Information S1 (Text S2) provides additional details on uncertainty propagation for SO_2 emissions.

We used a bootstrap approach (Efron & Tibshirani, 1986) to quantify how the distribution of measured Hg:SO_2 ratios (Table S1 in Supporting Information S1; Edwards et al., 2021) affects volcanic Hg emissions estimates. We estimated Hg emission flux for each volcano as the product of a Hg:SO_2 ratio randomly selected from available observations and the SO_2 flux for that volcano, sampled from within its uncertainty. We repeated this procedure over 10,000 iterations. Measured values were used for volcanoes with available Hg:SO_2 data. For volcanoes with no Hg measurements, we randomly selected Hg:SO_2 values from among all global measurements. Sites with available Hg:SO_2 measurements included 18 of the 194 volcanic SO_2 sources in the satellite record, representing 39% of total SO_2 emissions from passive degassing, 3% from explosive eruptions, and 60% from effusive

eruptions. Hg:SO_2 ratios were available from seven additional sites where the SO_2 flux was too small or transient for accurate satellite quantification. We included these seven Hg:SO_2 ratios in the bootstrap sampling distribution. We partitioned global Hg emissions among specific volcanic sites and events based on relative SO_2 emission magnitudes for use in global atmospheric modeling.

Prior work has estimated Hg emissions from volcanism by applying a uniform Hg:SO_2 value (Bagnato et al., 2015; Li et al., 2020). To generate a comparable result, we identified the central Hg:SO_2 ratio estimate from Bagnato et al. (2015) (7.8 μg g^{-1}) and combined this with the central estimate for SO_2 emissions. The difference between results from the bootstrap analysis and uniform scaling illustrates the effects of explicitly quantifying uncertainty in Hg:SO_2 ratios and SO_2 emissions in this work.

2.2. Global Atmospheric Modeling of Volcanic Hg Fate

We simulated the atmospheric transport and deposition of volcanic Hg emissions using the GEOS-Chem chemical transport model (v12.8, www.geos-chem.org). GEOS-Chem uses assimilated meteorological fields from the MERRA-2 reanalysis product and simulates atmospheric Hg chemistry using a state-of-the-science oxidation and reduction mechanism (Gelaro et al., 2017; Shah et al., 2021). The most recent version of the Hg model (Shah et al., 2021) incorporates gas-phase photolysis of oxidized Hg species and builds upon the multi-phase, two-stage oxidation mechanism developed in prior versions (Horowitz et al., 2017). This simulation bridges laboratory and computational chemistry results and has been extensively evaluated to ensure consistency with observational constraints (Horowitz et al., 2017; Shah et al., 2021). All simulations were conducted at a 2° × 2.5° horizontal resolution using a 72-level vertical model grid. Each simulation was initialized from a restart file following a 5-year spin-up, and volcanic Hg emissions were paired with the corresponding meteorological year.

We used the HEMCO emissions module (v2.2.0) (Keller et al., 2014) within GEOS-Chem to release Hg at specific altitudes for different volcanic events and evaluate the effects of plume injection altitude on the lifetime and dispersal of Hg released by eruptive volcanism. Emissions from effusive and explosive eruptions were released to a height corresponding to the upper third of the distance between the vent altitude and the uppermost extent of the volcanic plume, following previously established methods (Chin et al., 2000; Ge et al., 2016). Hg emissions from passive degassing were mixed into the planetary boundary layer following the standard scheme used for anthropogenic emissions (Lin & McElroy, 2010). This scheme does not account for passive releases from a few high emitting volcanoes that may result in buoyant plumes and high-altitude releases, but presently there is no standardized way to represent such phenomena in the model.

We performed separate 17-year global simulations (2005–end of 2021) for each category of volcanism (passive degassing, effusive eruptions, and explosive eruptions) and for two functionally defined Hg species (Hg^0 and Hg^{II}). This approach allows for sensitivity analysis of atmospheric concentrations and deposition to speciated emissions from a given process using source-receptor methods (Corbitt et al., 2011). We specified plume speciation based on average values simulated by Von Glasow (2010) over the 3 days following eruption (i.e., 8% [2%–10%] particulate bound Hg^{II}, 23% [7%–46%] gaseous Hg^{II}, and 69% [44%–91%] Hg^0). Hg^{II} species were initially specified as $HgCl_2$(g), for consistency with the Shah et al. (2021) benchmark.

2.3. Model Experiments Varying Plume Height and Hg Speciation at Two Sites

We conducted separate model experiments using GEOS-Chem to evaluate the effects of plume injection altitude and Hg speciation on the fate of volcanic Hg emissions. In each experiment (n = 576), we simulated an eruption emitting 100 Mg Hg over 1 day and tracked its dispersion for 6 months. The plume was released to one of six atmospheric pressure levels (945–18 hPa), and Hg speciation was specified as one of three gaseous Hg species (Hg^0, $HgCl_2$, $HgBr_2$) or one particulate species (Hg(II) chloride salts on sea salt aerosol). Eruptions were simulated at a mid-latitude volcano (Mount Saint Helens; 46.19°N, 122.20°W) and a tropical volcano (Mount Pinatubo; 15.14°N, 120.35°E) to evaluate effects from differences in tropopause height and atmospheric transport. Each experimental treatment was replicated over 12 start dates on the first day of each month.

2.4. Global Geochemical Box Modeling

We simulated the natural global Hg budget by forcing a 7-box geochemical model (Global Biogeochemical Box Model [GBBM]) (Amos et al., 2013, 2014) with the volcanic emissions estimated in this work to steady state

Table 1
Global Mercury Emissions From Volcanism[a]

Flux type	Year range	Active sites (n)	SO_2 (Tg a^{-1}) $\mu \pm \sigma$	Hg, traditional scaling[b] (Mg a^{-1}) $\mu \pm \sigma$	Hg, best estimate[c] (Mg a^{-1}) *Median* (*IQR*)
Passive degassing	2005–2021	106	20 ± 1.6	155 ± 109	211 (157–301)
Effusive eruptions	1979–2021	30	1.4 ± 0.4	11 ± 8.1	9.1 (5.5–17)
Explosive eruptions	1978–2021	119	1.3 ± 0.2	10 ± 7.5	12 (8.1–18)
All categories			23 ± 2.2	177 ± 125	232 (170–336)

[a]Emission magnitudes and uncertainties represent the temporal mean over the time range provided. [b]Global volcanic Hg emissions estimated using a uniform Hg:SO_2 ratio from Bagnato et al. (2015) (7.8 μg g^{-1}) and the central SO_2 emissions estimate from satellite data. [c]Global volcanic Hg emissions estimated using a bootstrap procedure for sampling the empirical distribution of Hg:SO_2 ratios and SO_2 emission fluxes from each volcano, over 10,000 iterations. IQR = interquartile range. Note that emissions are generally reported to two significant figures; three significant figures are reported where emissions exceed 100 Mg a^{-1}.

(Table S4 in Supporting Information S1). Model compartments included the atmosphere, three ocean compartments delineated by depth (surface, intermediate, deep), and three compartments for terrestrial vegetation and soils delineated by carbon turnover time (fast, slow, and protected). The model is defined as a system of first-order differential equations of the form:

$$\frac{dm}{dt} = \mathbf{K}m + s$$

in which m is a vector containing the mass in each of the seven reservoirs, s is a vector containing inputs to each reservoir and $\mathbf{K}$ is the 7×7 matrix of rate coefficients coupling each reservoir pair (Amos et al., 2013). We additionally included natural inputs of Hg from deep-sea hydrothermal vents (50 Mg a^{-1}) to the deep ocean based on Hg concentrations measured in vent fluid (4–10 pmol kg^{-1}) (Lamborg et al., 2006; Lee et al., 2015) and the upper range of flows to the deep ocean (1–4 × 10^{19} g a^{-1}, 1 Sverdrup) (Lamborg et al., 2006; Mottl, 2003).

3. Results and Discussion

3.1. Global Volcanic Emissions

Results of the bootstrap simulation suggest global volcanic Hg fluxes across all emission categories are 232 Mg a^{-1} (interquartile range = 170–336 Mg a^{-1}). Passive degassing (211 [157–301] Mg a^{-1}) accounts for 91% of emissions. Effusive (9.1 [5.5–17] Mg a^{-1}) and explosive (12 [8.1–18] Mg a^{-1}) eruptions make up the remaining 9% of volcanic emissions (Table 1). Uniform scaling of Hg:SO_2 ratios produces lower passive degassing estimates than the bootstrap analysis (155 ± 109 Mg a^{-1}; mean ± standard deviation) and comparable estimates for effusive and explosive eruptions (11 ± 8.1 and 10 ± 7.5 Mg a^{-1}, respectively; Table 1).

The bootstrap method ("Best Estimate," Table 1) better captures high-emitting sites that elevate the total Hg emissions relative to the uniform scaling method used in most past work ("Traditional Scaling," Table 1). Hg:SO_2 measurements exhibit a long-tailed distribution, implying that most volcanoes fall below the mean of the observed Hg:SO_2 distribution, while a few volcanoes emit at a much higher ratio. This distribution highlights the presence of a few "super-emitting" sites characterized by high Hg:SO_2 ratios that disproportionately affect global volcanic Hg emissions.

3.2. Greatest Volcanic Hg Releases in the Tropics and Mid-Latitude Northern Hemisphere

Most (75%) global volcanic Hg releases are concentrated in the tropics. Emissions of 67 Mg Hg a^{-1} are released in the Northern Hemisphere (NH) tropics (Equator–23.5°N) and 107 Mg Hg a^{-1} are released in the Southern Hemisphere (SH) tropics (Equator–23.5°S). These emissions undergo interhemispheric exchange during seasonal migration of the Intertropical Convergence Zone. This results in elevated mean tropical atmospheric Hg concentrations (+28%) and deposition (+61%) attributable to volcanic emissions compared to extratropical regions (Figure 1).

By contrast, the magnitude of volcanic Hg sources and associated atmospheric concentrations and deposition varies between the extratropical NH and SH (Figure S1 in Supporting Information S1). In the mid-latitude SH

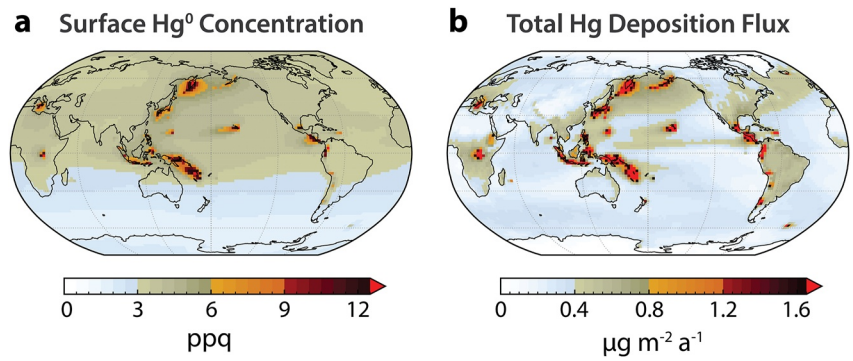

Figure 1. *Effects of volcanic mercury emissions on annual mean (2005–2022) concentrations and deposition*. Panel (a) shows surface-level atmospheric Hg^0 concentrations from primary volcanic Hg emissions. Panel (b) shows simulated net deposition flux (wet and dry). Simulations were conducted using the GEOS-Chem global atmospheric Hg model (v12.8, Shah et al., 2021) forced with daily volcanic Hg emissions (2005–2022) from three eruption categories (passive degassing, effusive eruptions, and explosive eruptions). Light red represents values above 20 ppq and 5 μg m^{-2} a^{-1} for panels (a, b), respectively.

(23.5°S–66.5°S), only 6.2 Mg a^{-1} of volcanic Hg is emitted compared to 51 Mg a^{-1} in the mid-latitude NH (23.5°N–66.5°N). Negligible volcanic Hg emissions occur in polar regions (<0.1 Mg a^{-1}, Figure S1 in Supporting Information S1).

These differences propagate to atmospheric concentrations and deposition due to the relatively long timescales required for extratropical interhemispheric mixing. Extratropical Hg emissions largely remain in their hemisphere of origin because the lifetime of Hg against deposition (τ = 5.5 months in troposphere, Shah et al., 2021) is shorter than the timescales required for interhemispheric transport (~1–1.5 years) (Geller et al., 1997; Jacob et al., 1987). For example, volcanic Hg emissions cause surface-level (0–320 m) atmospheric Hg concentrations to be 83% greater in the extratropical NH than in the extratropical SH (Figure 1a).

Volcanism disproportionately affects total atmospheric Hg concentrations and deposition in several regions (Figure 1). For example, Kamchatka, Japan, Melanesia, Central America, Central Africa, Hawaii, and the Mediterranean all have volcanic Hg deposition levels that exceed 5 μg m^{-2} a^{-1} (light red in Figure 1b). This occurs even though the total magnitude of volcanic Hg emissions (232 Mg a^{-1}) is approximately an order of magnitude less than contemporary anthropogenic emissions of ~2,000 Mg a^{-1} (Shah et al., 2021; Streets et al., 2019).

3.3. Large Temporal Variability in Eruptive Hg Emissions

Eruptive volcanic emissions show much greater interannual variability than passive degassing. Over the last several decades, Hg emissions from explosive eruptions have varied by approximately three orders of magnitude from year to year. Between 1979 and 2022, the lowest eruptive Hg releases occurred in 1987 when eruptions at Klyuchevskoy (Russia) and Nyamuragira (Democratic Republic of the Congo) released <0.1 [0–0.1] Mg Hg a^{-1}. Highest eruptive Hg emissions occurred in 1991 (79 [44–160] Mg a^{-1}) when Mount Pinatubo in the Philippines released an estimated 55 [23–120] Mg Hg (Table S5 in Supporting Information S1).

The impacts of volcanic Hg emissions on atmospheric Hg concentrations and deposition are greatest in the days to weeks following effusive and explosive eruptions. Modeling suggests that individual explosive eruptions since 2005 have enhanced Hg concentrations by >200 ppq during the month of the eruption within the 2° × 2.5° area surrounding the vent. This represents an approximate doubling of Hg mixing ratios relative to the background atmosphere, though ventilation and high plume injection altitudes mitigate near-field deposition impacts. In comparison, large effusive eruptions may cause greater near-field deposition because of lower injection altitudes and longer lasting eruptive events. We estimate that the largest effusive eruptions from Kīlauea (Hawaii, USA) increased atmospheric Hg concentrations by >300 ppq and deposition by 33 μg m^{-2} in June 2018, and annual deposition increased by 91 μg m^{-2} during 2018–2019.

Effects of variability in volcanic Hg emissions on atmospheric Hg concentrations and deposition should be considered when establishing new stations for monitoring how reductions in anthropogenic Hg emissions affect atmospheric Hg concentrations. This question is essential for evaluating the effectiveness of the global Minamata

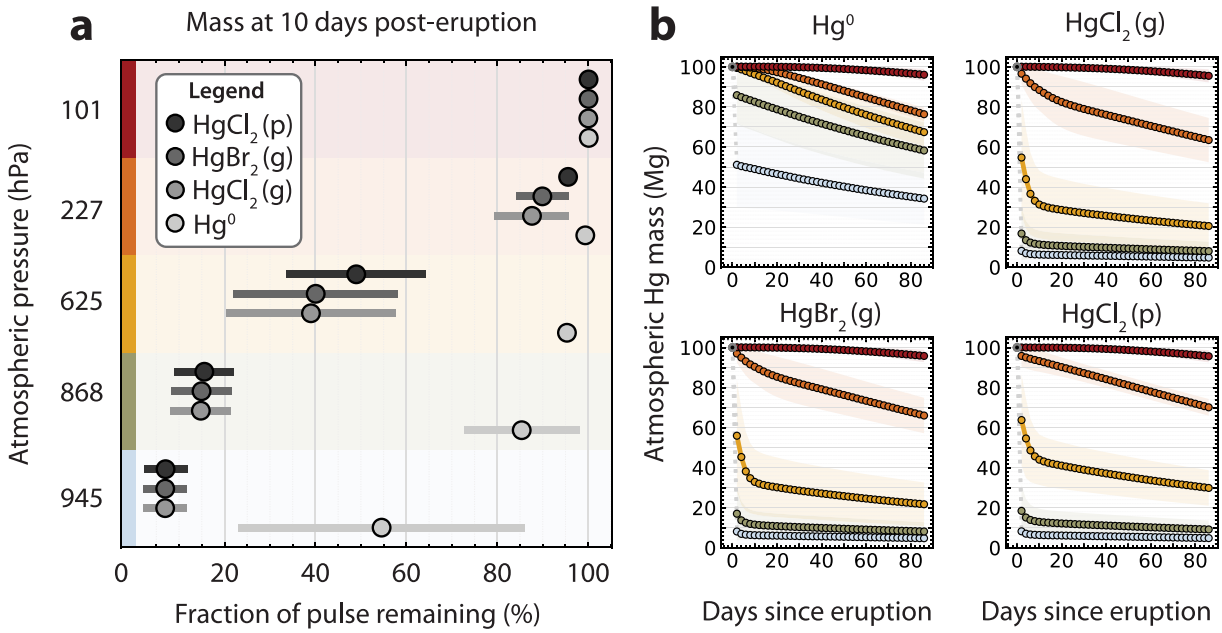

Figure 2. *Fate of a 100* Mg *pulse of volcanic Hg released to the atmosphere*. Panel (a) shows the effects of varying plume injection altitude on the fraction of initial mass remaining 10 days after the pulse was released. Panel (b) shows the effects of differences in Hg speciation of the initial pulse on atmospheric Hg mass trends over the 3 months following eruption for each emitted Hg species (subpanels) and pressure level (point color). All experiments were conducted using the GEOS-Chem atmospheric Hg model (v12.8) (Shah et al., 2021). (a) Error bars and (b) shaded regions show variability (1σ) based on release location (Pinabuto and Mt. St. Helens) and eruption date. Oxidized Hg species are annotated as gaseous (g) or particulate (p).

Convention on Mercury (Pirrone et al., 2013). For example, volcanic Hg emissions drive interannual variability (1σ) of up to 9.6% of annual mean atmospheric Hg concentrations at existing monitoring sites (Table S3 in Supporting Information S1). Volcanic emissions also produce atmospheric Hg trends ranging from −0.49% a^{-1} (AMNet HI00; Hawaii, USA) to +0.42% a^{-1} (GMOS MIN; Minamata, Japan) from 2005 to 2022 (Table S3 in Supporting Information S1), which is 20%–40% of the −1.2% a^{-1} to −2.1% a^{-1} trend observed since the 1990s at mid-latitude NH sites (Zhang et al., 2016). Variability in volcanic Hg emissions may therefore confound interpretation of atmospheric Hg trends in response to shifts in anthropogenic emissions at some monitoring sites and should be considered when interpreting temporal trends.

3.4. Atmospheric Hg Lifetime Dictated by Plume Injection Altitude for Eruptive Emissions

Volcanic eruptions can introduce Hg to the upper troposphere and lower stratosphere, thereby extending its lifetime in the atmosphere. Model experiments show much lower (10–15x) initial deposition of oxidized Hg in plumes released to 101 hPa (~16 km) from Mt. Pinatubo (tropics) and Mt. St. Helens (mid-latitude NH) relative to those released near the surface (945 hPa = ~0.6 km). We found >90% of oxidized Hg released to 945 hPa was re-deposited within 10 days, compared to <60% at 625 hPa (~3.9 km) and 13% at 227 hPa (11 km) (Figure 2). This pattern reflects decreased scavenging by precipitation with higher altitude throughout the troposphere.

After ~10 days, modeling results show a pronounced "elbow" in the atmospheric loss rate (Figure 2b). This occurs when the volcanic plume of oxidized Hg has been either scavenged by precipitation and particle settling, or it has undergone conversion to Hg^0 via aerosol uptake of $HgCl_{2(g)}$ and $HgBr_{2(g)}$, followed by photoreduction of aqueous organic aerosol ($Hg^{II}_{P(org)}$) to Hg^0 (Shah et al., 2021). Atmospheric Hg remaining after 10 days generally follows first-order loss with an average atmospheric lifetime of 5.3 months across model experiments. This result is consistent with the overall tropospheric lifetime of 5.5 months from Shah et al. (2021) and observationally constrained values of 4–7 months (De Simone et al., 2014; Holmes et al., 2010; Horowitz et al., 2017).

The volcanic plume injection altitude of Hg^0 is less important for the atmospheric lifetime because it is sparingly soluble and is not scavenged by precipitation. Approximately half of Hg^0 released near the surface (945 hPa) in model experiments was lost within 10 days (Figure 2). We found only small differences between volcanic plume

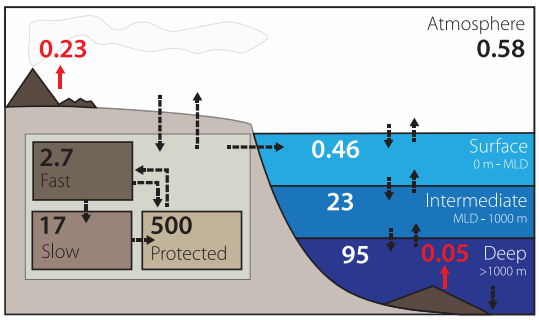

Figure 3. *Natural global mercury (Hg) budget prior to human influence*. Simulated Hg mass (Gg; black and white) in major reservoirs is calculated at steady state using the seven-compartment global biogeochemical mercury model (Amos et al., 2013, 2014). Updated fluxes from the model are provided in Table S4 in Supporting Information S1. Geogenic emissions (red) are based on the central estimate for all categories of subaerial volcanism (passive degassing, effusive eruptions, and explosive eruptions) presented in this work (0.23 Gg a^{-1}), and from submarine hydrothermal activity (0.05 Gg a^{-1}). Ocean compartments are annotated with their corresponding depth scale, with a global average mixed layer depth of ∼54 m (Montégut, 2004).

injection at 625 hPa (∼3.9 km) and 227 hPa (∼11 km) for atmospheric Hg^0 removal after 10 days (4% and 1%, respectively).

Volcanic Hg in plumes reaching the stratosphere exhibit substantially longer lifetimes against deposition. Minimal losses (<5%) were observed in model experiments for both oxidized Hg and Hg^0 at the 101 hPa (16 km) level, with greater losses observed at Pinatubo (tropics) owing to the higher position of the low-latitude tropopause compared to Mt. St. Helens (mid-latitude NH). The deposition lifetime of Hg may increase with altitude above the tropopause, where vertical mass transport is slow. No appreciable atmospheric Hg removal was observed over the six months following release for any of the Hg species emitted to the highest altitudes (18 hPa; 27 km), which may be relevant for the very largest eruptions emitting material to 40–57 km (Holasek et al., 1996; Proud et al., 2022).

In summary, these results reinforce that the atmospheric lifetime of volcanic Hg emissions is primarily controlled by Hg speciation, but plume injection altitude is most important for explosive eruptions. Explosive eruptions inject Hg to the upper troposphere and stratosphere, where rates of scavenging by precipitation and settling particles are slow and Hg emissions are likely to undergo chemical processing with background air masses before removal. In contrast, a large proportion of near-surface releases from passive degassing deposit close to the source, particularly when Hg is emitted in oxidized forms. Additional constraints on factors controlling the lifetime of Hg in volcanic plumes may be gained though mechanistic studies on Hg sorption and removal by sulfate-rich volcanic ash (Koenig et al., 2023).

3.5. Natural Global Biogeochemical Hg Cycle

Natural Hg releases estimated in this study using the GBBM support a pre-anthropogenic atmospheric Hg reservoir of 580 Mg (IQR: 410–820 Mg, Figure 3) compared to 4,000 Mg estimated for 2015 (Shah et al., 2021). Hg releases from deep-ocean hydrothermal vents (50 Mg a^{-1}) account for an estimated 5% of the natural atmospheric reservoir and 8% of the surface ocean to 1,000 m depth. This reinforces that the natural atmospheric Hg budget is primarily driven by subaerial volcanism.

The 2013–2015 atmospheric reservoir (4,000 Mg) simulated in GEOS-Chem (Shah et al., 2021) corresponds to an approximately 7-fold (IQR: 4.9–9.8) enrichment above the natural level simulated using the GBBM. Enrichment factors for Hg based on sediment and peat records have been reviewed extensively in prior work (Amos et al., 2015; Biester et al., 2007; Cooke et al., 2020; Li et al., 2020). These records indicate that Hg accumulation rates have increased by a factor of ∼5–13 in the modern era (1990–2010) compared to pre-1450 levels. Archives focusing on shorter records since the industrial revolution (ca. 1850) to maximum 20th century deposition levels demonstrate lower enrichment factors of approximately 3–5, and mainly reflect shifts in anthropogenic Hg releases over this period (Fitzgerald et al., 1998; Lamborg et al., 2002).

4. Conclusions

Accounting for the long-tailed distribution of observed Hg:SO_2 ratios in volcanic plumes results in higher volcanic Hg flux estimates (232 Mg a^{-1}) compared to the traditionally used method of uniformly scaling Hg:SO_2 ratios (177 Mg a^{-1}) (Bagnato et al., 2015). This implies that a few volcanoes with high Hg:SO_2 contribute disproportionately to the global total and should be identified and monitored to better constrain spatial and temporal release estimates. Cumulative SO_2 emissions are strongly impacted by only a few sites, indicating that a large fraction of global Hg emissions could be continuously observed through directed measurement. Eruptive emissions have varied by three orders of magnitude over the last four decades but are less important than passive degassing on an annualized basis (21 vs. 211 Mg a^{-1}). Interannual variability in volcanic emissions may obscure atmospheric trends forced by anthropogenic emissions at certain monitoring sites. Accounting for contributions of volcanic Hg at both present and future monitoring locations is therefore important for long-term trend analysis. For example, past work shows that proximity to volcanos in southwest Alaska is an important predictor of both plankton methylmercury concentrations (Bartz et al., 2023) and Hg isotopic signatures in lake trout (Lepak et al., 2015).

For explosive eruptions, plume injection altitude controls the atmospheric lifetime of emitted Hg because deposition declines with plume altitude in the days following eruption. For passive degassing and effusive eruptions, Hg speciation in the volcanic plume is most important for the atmospheric lifetime of Hg emissions. The highest concentrations and deposition of volcanic Hg emissions occur in the tropics. More volcanic Hg is present in the extratropical NH atmosphere compared with the extratropical SH. This reflects both higher emissions and extended timescales of extratropical interhemispheric exchange that are longer than the lifetime of tropospheric Hg against deposition. Finally, the present-day (2013–2015) atmospheric Hg reservoir appears to be ∼7-fold (IQR: 4.9–9.8) larger than the natural reservoir based on volcanic release estimates.

This work provides an approach for space-based observation of volcanic Hg emissions and a template for studying the fate of volcanic Hg using mechanistic and dynamical models. Additional measurements of Hg speciation in magmatic gases, which exhibit wide variation in temperature, initial oxidation state, and oxidant concentrations would further improve and constrain volcanic Hg emissions estimates. Ideally, such research would focus on improving mechanistic understanding of how Hg:SO_2 relationships vary with tectonic setting and style of volcanism.

Conflict of Interest

The authors declare no conflicts of interest relevant to this study.

Data Availability Statement

Mercury emission files and model output are available on the Harvard Dataverse (Geyman, 2023b). Code written to generate emission files and analyze model output is archived on Zenodo (Geyman, 2023a). SO_2 emissions from explosive and effusive eruptions were downloaded from the MSVOLSO2L4 database (Carn, 2022). SO_2 emissions from passive degassing were downloaded from (https://so2.gsfc.nasa.gov/measures.html).

Acknowledgments
We thank J. Gačnik and one anonymous reviewer, whose suggestions helped improve and clarify this manuscript. V. Shah provided useful discussions during study preparation. Financial support for this work was provided by the U.S. National Science Foundation (Awards 2210173 and 2108452).

References

Aiuppa, A., Bagnato, E., Witt, M. L. I., Mather, T. A., Parello, F., Pyle, D. M., & Martin, R. S. (2007). Real-time simultaneous detection of volcanic Hg and SO_2 at La Fossa Crater, Vulcano (Aeolian Islands, Sicily). *Geophysical Research Letters*, *34*(21), L21307. https://doi.org/10.1029/2007GL030762

Amos, H. M., Jacob, D. J., Kocman, D., Horowitz, H. M., Zhang, Y., Dutkiewicz, S., et al. (2014). Global biogeochemical implications of mercury discharges from rivers and sediment burial. *Environmental Science & Technology*, *48*(16), 9514–9522. https://doi.org/10.1021/es502134t

Amos, H. M., Jacob, D. J., Streets, D. G., & Sunderland, E. M. (2013). Legacy impacts of all-time anthropogenic emissions on the global mercury cycle. *Global Biogeochemical Cycles*, *27*(2), 410–421. https://doi.org/10.1002/gbc.20040

Amos, H. M., Sonke, J. E., Obrist, D., Robins, N., Hagan, N., Horowitz, H. M., et al. (2015). Observational and modeling constraints on global anthropogenic enrichment of mercury. *Environmental Science & Technology*, *49*(7), 4036–4047. https://doi.org/10.1021/es5058665

Andres, R. J., & Kasgnoc, A. D. (1998). A time-averaged inventory of subaerial volcanic sulfur emissions. *Journal of Geophysical Research*, *103*(D19), 251–276. https://doi.org/10.1029/98JD02091

Bagnato, E., Aiuppa, A., Parello, F., Allard, P., Shinohara, H., Liuzzo, M., & Giudice, G. (2011). New clues on the contribution of Earth's volcanism to the global mercury cycle. *Bulletin of Volcanology*, *73*(5), 497–510. https://doi.org/10.1007/s00445-010-0419-y

Bagnato, E., Aiuppa, A., Parello, F., Calabrese, S., D'Alessandro, W., Mather, T. A., et al. (2007). Degassing of gaseous (elemental and reactive) and particulate mercury from Mount Etna volcano (Southern Italy). *Atmospheric Environment*, *41*(35), 7377–7388. https://doi.org/10.1016/j.atmosenv.2007.05.060

Bagnato, E., Tamburello, G., Avard, G., Martinez-Cruz, M., Enrico, M., Fu, X., et al. (2015). Mercury fluxes from volcanic and geothermal sources: An update. *Geological Society, London, Special Publications*, *410*(1), 263–285. https://doi.org/10.1144/SP410.2

Bartz, K. K., Hannam, M. P., Wilson, T. L., Lepak, R. F., Ogorek, J. M., Young, D. B., et al. (2023). Understanding drivers of mercury in lake trout (Salvelinus namaycush), a top-predator fish in southwest Alaska's parklands. *Environmental Pollution*, *330*, 121678. https://doi.org/10.1016/j.envpol.2023.121678

Biester, H., Bindler, R., Martinez-Cortizas, A., & Engstrom, D. R. (2007). Modeling the past atmospheric deposition of mercury using natural archives. *Environmental Science & Technology*, *41*(14), 4851–4860. https://doi.org/10.1021/es0704232

Carn, S. A. (2022). Multi-satellite volcanic sulfur dioxide L4 long-term global database V4, Greenbelt, MD, USA [Dataset]. Goddard Earth Science Data and Information Services Center (GES DISC). https://doi.org/10.5067/MEASURES/SO2/DATA405

Carn, S. A., Clarisse, L., & Prata, A. J. (2016). Multi-decadal satellite measurements of global volcanic degassing. *Journal of Volcanology and Geothermal Research*, *311*, 99–134. https://doi.org/10.1016/j.jvolgeores.2016.01.002

Carn, S. A., Fioletov, V. E., McLinden, C. A., Li, C., & Krotkov, N. A. (2017). A decade of global volcanic SO_2 emissions measured from space. *Scientific Reports*, *7*(1), 44095. https://doi.org/10.1038/srep44095

Chin, M., Rood, R. B., Lin, S. J., Müller, J. F., & Thompson, A. M. (2000). Atmospheric sulfur cycle simulated in the global model GOCART: Model description and global properties. *Journal of Geophysical Research*, *105*(D20), 24671–24687. https://doi.org/10.1029/2000JD900384

Cooke, C. A., Martínez-Cortizas, A., Bindler, R., & Sexauer Gustin, M. (2020). Environmental archives of atmospheric Hg deposition – A review. *Science of the Total Environment*, *709*, 134800. https://doi.org/10.1016/j.scitotenv.2019.134800

Corbitt, E. S., Jacob, D. J., Holmes, C. D., Streets, D. G., & Sunderland, E. M. (2011). Global source-receptor relationships for mercury deposition under present-day and 2050 emissions scenarios. *Environmental Science & Technology*, *45*(24), 10477–10484. https://doi.org/10.1021/es202496y

Dedeurwaerder, H., Decadt, G., & Baeyens, W. (1982). Estimations of mercury fluxes emitted by Mount Etna volcano. *Bulletin Volcanologique*, *45*(3), 191–196. https://doi.org/10.1007/BF02597729

De Simone, F., Gencarelli, C. N., Hedgecock, I. M., & Pirrone, N. (2014). Global atmospheric cycle of mercury: A model study on the impact of oxidation mechanisms. *Environmental Science and Pollution Research*, *21*(6), 4110–4123. https://doi.org/10.1007/s11356-013-2451-x

Edwards, B. A., Kushner, D. S., Outridge, P. M., & Wang, F. (2021). Fifty years of volcanic mercury emission research: Knowledge gaps and future directions. *Science of the Total Environment*, *757*, 143800. https://doi.org/10.1016/j.scitotenv.2020.143800

Efron, B., & Tibshirani, R. (1986). Bootstrap methods for standard Errors, confidence Intervals, and other measures of statistical accuracy. *Statistical Science*, *1*(1), 54–75. https://doi.org/10.1214/ss/1177013815

Ferrara, R., Mazzolai, B., Lanzillotta, E., Nucaro, E., & Pirrone, N. (2000). Volcanoes as emission sources of atmospheric mercury in the Mediterranean basin. *The Science of the Total Environment*, *259*(1–3), 183–190. https://doi.org/10.1016/s0048-9697(00)00581-7

Fioletov, V. E., McLinden, C. A., Griffin, D., Abboud, I., Krotkov, N., Leonard, P. J. T., et al. (2023). Version 2 of the global catalogue of large anthropogenic and volcanic SO_2 sources and emissions derived from satellite measurements. *Earth System Science Data*, *15*(1), 75–93. https://doi.org/10.5194/essd-15-75-2023

Fitzgerald, W. F., Engstrom, D. R., Mason, R. P., & Nater, E. A. (1998). The case for atmospheric Mercury contamination in remote areas. *Environmental Science & Technology*, *32*(1), 1–7. https://doi.org/10.1021/es970284w

Ge, C., Wang, J., Carn, S., Yang, K., Ginoux, P., & Krotkov, N. (2016). Satellite-based global volcanic SO_2 emissions and sulfate direct radiative forcing during 2005-2012. *Journal of Geophysical Research: Atmospheres*, *121*(7), 3446–3464. https://doi.org/10.1002/2015JD023134

Gelaro, R., McCarty, W., Suárez, M. J., Todling, R., Molod, A., Takacs, L., et al. (2017). The modern-era retrospective analysis for research and applications, version 2 (MERRA-2). *Journal of Climate*, *30*(14), 5419–5454. https://doi.org/10.1175/JCLI-D-16-0758.1

Geller, L. S., Elkins, J. W., Lobert, J. M., Clarke, A. D., Hurst, D. F., Butler, J. H., & Myers, R. C. (1997). Tropospheric SF_6: Observed latitudinal distribution and trends, derived emissions and interhemispheric exchange time. *Geophysical Research Letters*, *24*(6), 675–678. https://doi.org/10.1029/97GL00523

Geyman, B. (2023a). bgeyman/global-volcanic-hg: Reproduction code (v1.1) [Software]. Zenodo. https://doi.org/10.5281/zenodo.8317654

Geyman, B. (2023b). Replication data for: Impacts of volcanic emissions on the global biogeochemical mercury cycle: Insights from satellite observations and chemical transport modeling [Dataset]. Harvard Dataverse, V2. https://doi.org/10.7910/DVN/KHP4KK

Gratz, L. E., Ambrose, J. L., Jaffe, D. A., Shah, V., Jaeglé, L., Stutz, J., et al. (2015). Oxidation of mercury by bromine in the subtropical Pacific free troposphere. *Geophysical Research Letters*, *42*(23), 10494–10502. https://doi.org/10.1002/2015GL066645

Holasek, R. E., Self, S., & Woods, A. W. (1996). Satellite observations and interpretation of the 1991 Mount Pinatubo eruption plumes. *Journal of Geophysical Research*, *101*(B12), 27635–27655. https://doi.org/10.1029/96JB01179

Holmes, C. D., Jacob, D. J., Corbitt, E. S., Mao, J., Yang, X., Talbot, R., & Slemr, F. (2010). Global atmospheric model for mercury including oxidation by bromine atoms. *Atmospheric Chemistry and Physics*, *10*(24), 12037–12057. https://doi.org/10.5194/acp-10-12037-2010

Horowitz, H. M., Jacob, D. J., Zhang, Y., Dibble, T. S., Slemr, F., Amos, H. M., et al. (2017). A new mechanism for atmospheric mercury redox chemistry: Implications for the global mercury budget. *Atmospheric Chemistry and Physics*, *17*(10), 6353–6371. https://doi.org/10.5194/acp-17-6353-2017

Jacob, D. J., Prather, M. J., Wofsy, S. C., & McElroy, M. B. (1987). Atmospheric distribution of ^{85}Kr simulated with a general circulation model. *Journal of Geophysical Research*, *92*(D6), 6614–6626. https://doi.org/10.1029/JD092iD06p06614

Keller, C. A., Long, M. S., Yantosca, R. M., Da Silva, A. M., Pawson, S., & Jacob, D. J. (2014). HEMCO v1.0: A versatile, ESMF-compliant component for calculating emissions in atmospheric models. *Geoscientific Model Development*, *7*(4), 1409–1417. https://doi.org/10.5194/gmd-7-1409-2014

Koenig, A. M., Magand, O., Rose, C., Di Muro, A., Miyazaki, Y., Colomb, A., et al. (2023). Observed in-plume gaseous elemental mercury depletion suggests significant mercury scavenging by volcanic aerosols. *Environmental Sciences: Atmosphere*. https://doi.org/10.1039/D3EA00063J

Lamborg, C. H., Fitzgerald, W. F., Damman, A. W. H., Benoit, J. M., Balcom, P. H., & Engstrom, D. R. (2002). Modern and historic atmospheric mercury fluxes in both hemispheres: Global and regional mercury cycling implications. *Global Biogeochemical Cycles*, *16*(4), 51-1–51-11. https://doi.org/10.1029/2001GB001847

Lamborg, C. H., Von Damm, K. L., Fitzgerald, W. F., Hammerschmidt, C. R., & Zierenberg, R. (2006). Mercury and monomethylmercury in fluids from Sea Cliff submarine hydrothermal field, Gorda Ridge. *Geophysical Research Letters*, *33*(17), L17606. https://doi.org/10.1029/2006GL026321

Lee, S., Kim, S.-J., Ju, S.-J., Pak, S.-J., Son, S.-K., Yang, J., & Han, S. (2015). Mercury accumulation in hydrothermal vent mollusks from the southern Tonga Arc, southwestern Pacific Ocean. *Chemosphere*, *127*, 246–253. https://doi.org/10.1016/j.chemosphere.2015.01.006

Lepak, R. F., Yin, R., Krabbenhoft, D. P., Ogorek, J. M., Dewild, J. F., Holsen, T. M., & Hurley, J. P. (2015). Use of stable Isotope signatures to determine mercury sources in the Great Lakes. *Environmental Science & Technology Letters*, *2*(12), 335–341. https://doi.org/10.1021/acs.estlett.5b00277

Li, C., Sonke, J. E., Le Roux, G., Piotrowska, N., Van der Putten, N., Roberts, S. J., et al. (2020). Unequal anthropogenic enrichment of mercury in Earth's Northern and Southern Hemispheres. *ACS Earth and Space Chemistry*, *4*(11), 2073–2081. https://doi.org/10.1021/acsearthspacechem.0c00220

Lin, J.-T., & McElroy, M. B. (2010). Impacts of boundary layer mixing on pollutant vertical profiles in the lower troposphere: Implications to satellite remote sensing. *Atmospheric Environment*, *44*(14), 1726–1739. https://doi.org/10.1016/j.atmosenv.2010.02.009

Montégut, C. (2004). Mixed layer depth over the global ocean: An examination of profile data and a profile-based climatology. *Journal of Geophysical Research*, *109*(C12), C12003. https://doi.org/10.1029/2004JC002378

Mottl, M. J. (2003). Partitioning of energy and mass fluxes between mid-ocean ridge axes and flanks at high and low temperature. In P. E. Halbach, V. Tunnicliffe, & J. R. Hein (Eds.), *Energy and mass transfer in marine hydrothermal systems* (pp. 271–286). Dahlem University Press.

Nriagu, J. O. (1989). A global assessment of natural sources of atmospheric trace metals. *Nature*, *338*(6210), 47–49. https://doi.org/10.1038/338047a0

Obrist, D., Kirk, J. L., Zhang, L., Sunderland, E. M., Jiskra, M., & Selin, N. E. (2018). A review of global environmental mercury processes in response to human and natural perturbations: Changes of emissions, climate, and land use. *Ambio*, *47*(2), 116–140. https://doi.org/10.1007/s13280-017-1004-9

Pirrone, N., Aas, W., Cinnirella, S., Ebinghaus, R., Hedgecock, I. M., Pacyna, J., et al. (2013). Toward the next generation of air quality monitoring: Mercury. *Atmospheric Environment*, *80*, 599–611. https://doi.org/10.1016/j.atmosenv.2013.06.053

Proud, S. R., Prata, A. T., & Schmauß, S. (2022). The January 2022 eruption of Hunga Tonga-Hunga Ha'apai volcano reached the mesosphere. *Science*, *378*(6619), 554–557. https://doi.org/10.1126/science.abo4076

Pyle, D. M., & Mather, T. A. (2003). The importance of volcanic emissions for the global atmospheric mercury cycle. *Atmospheric Environment*, *37*(36), 5115–5124. https://doi.org/10.1016/j.atmosenv.2003.07.011

Shah, V., Jacob, D. J., Thackray, C. P., Wang, X., Sunderland, E. M., Dibble, T. S., et al. (2021). Improved mechanistic model of the atmospheric redox chemistry of mercury. *Environmental Science & Technology*, *55*(21), 14445–14456. https://doi.org/10.1021/acs.est.1c03160

Streets, D. G., Horowitz, H. M., Lu, Z., Levin, L., Thackray, C. P., & Sunderland, E. M. (2019). Global and regional trends in mercury emissions and concentrations, 2010–2015. *Atmospheric Environment*, *201*, 417–427. https://doi.org/10.1016/j.atmosenv.2018.12.031

Varekamp, J. C., & Buseck, P. R. (1981). Mercury emissions from Mount St Helens during September 1980. *Nature*, *293*(5833), 555–556. https://doi.org/10.1038/293555a0

Von Glasow, R. (2010). Atmospheric chemistry in volcanic plumes. *Proceedings of the National Academy of Sciences of the United States of America*, *107*(15), 6594–6599. https://doi.org/10.1073/pnas.0913164107

Witt, M. L. I., Fischer, T. P., Pyle, D. M., Yang, T. F., & Zellmer, G. F. (2008a). Fumarole compositions and mercury emissions from the Tatun Volcanic Field, Taiwan: Results from multi-component gas analyser, portable mercury spectrometer and direct sampling techniques. *Journal of Volcanology and Geothermal Research*, *178*(4), 636–643. https://doi.org/10.1016/j.jvolgeores.2008.06.035

Witt, M. L. I., Mather, T. A., Pyle, D. M., Aiuppa, A., Bagnato, E., & Tsanev, V. I. (2008b). Mercury and halogen emissions from Masaya and Telica volcanoes, Nicaragua. *Journal of Geophysical Research*, *113*(6), 1–15. https://doi.org/10.1029/2007JB005401

Zambardi, T., Sonke, J. E., Toutain, J. P., Sortino, F., & Shinohara, H. (2009). Mercury emissions and stable isotopic compositions at Vulcano Island (Italy). *Earth and Planetary Science Letters*, *277*(1–2), 236–243. https://doi.org/10.1016/j.epsl.2008.10.023

Zhang, Y., Jacob, D. J., Horowitz, H. M., Chen, L., Amos, H. M., Krabbenhoft, D. P., et al. (2016). Observed decrease in atmospheric mercury explained by global decline in anthropogenic emissions. *Proceedings of the National Academy of Sciences of the United States of America*, *113*(3), 526–531. https://doi.org/10.1073/pnas.1516312113

References From the Supporting Information

Allard, P., Aiuppa, A., Bani, P., Métrich, N., Bertagnini, A., Gauthier, P.-J., et al. (2016). Prodigious emission rates and magma degassing budget of major, trace and radioactive volatile species from Ambrym basaltic volcano, Vanuatu island Arc. *Journal of Volcanology and Geothermal Research*, *322*, 119–143. https://doi.org/10.1016/j.jvolgeores.2015.10.004

Bagnato, E., Allard, P., Parello, F., Aiuppa, A., Calabrese, S., & Hammouya, G. (2009). Mercury gas emissions from La Soufrière volcano, Guadeloupe Island (lesser Antilles). *Chemical Geology*, *266*(3–4), 267–273. https://doi.org/10.1016/j.chemgeo.2009.06.011

Bagnato, E., Parello, F., Valenza, M., & Caliro, S. (2009). Mercury content and speciation in the Phlegrean Fields volcanic complex: Evidence from hydrothermal system and fumaroles. *Journal of Volcanology and Geothermal Research*, *187*(3–4), 250–260. https://doi.org/10.1016/j.jvolgeores.2009.09.010

Friedli, H. R., Radke, L. F., Prescott, R., Li, P., Woo, J. H., & Carmichael, G. R. (2004). Mercury in the atmosphere around Japan, Korea, and China as observed during the 2001 ACE-Asia field campaign: Measurements, distributions, sources, and implications. *Journal of Geophysical Research*, *109*(19), D19S25. https://doi.org/10.1029/2003JD004244

Gagliano, A. L., Calabrese, S., Daskalopoulou, K., Cabassi, J., Capecchiacci, F., Tassi, F., et al. (2019). Degassing and cycling of mercury at Nisyros volcano (Greece). *Geofluids*, *2019*, 1–18. https://doi.org/10.1155/2019/4783514

Gay, D. A., Schmeltz, D., Prestbo, E., Olson, M., Sharac, T., & Tordon, R. (2013). Atmospheric chemistry and physics the atmospheric mercury network: Measurement and initial examination of an ongoing atmospheric mercury record across North America. *Atmospheric Chemistry and Physics*, *13*(22), 11339–11349. https://doi.org/10.5194/acp-13-11339-2013

Jaffe, D., Prestbo, E., Swartzendruber, P., Weiss-Penzias, P., Kato, S., Takami, A., et al. (2005). Export of atmospheric mercury from Asia. *Atmospheric Environment*, *39*(17), 3029–3038. https://doi.org/10.1016/j.atmosenv.2005.01.030

Kyle, P. R., Meeker, K., & Finnegan, D. (1990). Emission rates of sulfur dioxide, trace gases and metals from Mount Erebus, Antarctica. *Geophysical Research Letters*, *17*(12), 2125–2128. https://doi.org/10.1029/GL017i012p02125

Mather, T. A., Witt, M. L. I., Pyle, D. M., Quayle, B. M., Aiuppa, A., Bagnato, E., et al. (2012). Halogens and trace metal emissions from the ongoing 2008 summit eruption of Kīlauea volcano, Hawaïi. *Geochimica et Cosmochimica Acta*, *83*, 292–323. https://doi.org/10.1016/j.gca.2011.11.029

Schiavo, B., Morton-Bermea, O., Salgado-Martinez, E., Arellano, J., & Hernández-Álvarez, E. (2020). Estimates of mercury flux and temporal variability of Hg/SO_2 ratio in the plume of Popocatépetl volcano (Mexico). *Journal of South American Earth Sciences*, *101*, 102614. https://doi.org/10.1016/j.jsames.2020.102614

Siegel, B. Z., & Siegel, S. M. (1987). Hawaiian volcanoes and the biogeology of mercury. *U. S. Geological Survey Professional Paper*, *1350*(1), 827–839. https://doi.org/10.3133/pp1350

Sprovieri, F., Pirrone, N., Bencardino, M., D'Amore, F., Carbone, F., Cinnirella, S., et al. (2016). Atmospheric mercury concentrations observed at ground-based monitoring sites globally distributed in the framework of the GMOS network. *Atmospheric Chemistry and Physics*, *16*(18), 11915–11935. https://doi.org/10.5194/acp-16-11915-2016

St. Louis, V. L., Graydon, J. A., Lehnherr, I., Amos, H. M., Sunderland, E. M., St. Pierre, K. A., et al. (2019). Atmospheric concentrations and wet/dry loadings of mercury at the remote experimental lakes area, northwestern Ontario, Canada. *Environmental Science & Technology*, *53*(14), 8017–8026. https://doi.org/10.1021/acs.est.9b01338

Varekamp, J. C., & Buseck, P. R. (1986). Global mercury flux from volcanic and geothermal sources. *Applied Geochemistry*, *1*(1), 65–73. https://doi.org/10.1016/0883-2927(86)90038-7

Wardell, L. J., Kyle, P. R., & Counce, D. (2008). Volcanic emissions of metals and halogens from White Island (New Zealand) and Erebus volcano (Antarctica) determined with chemical traps. *Journal of Volcanology and Geothermal Research*, *177*(3), 734–742. https://doi.org/10.1016/j.jvolgeores.2007.07.007

Yamakawa, A., Takami, A., Takeda, Y., Kato, S., & Kajii, Y. (2019). Emerging investigator series: Investigation of mercury emission sources using Hg isotopic compositions of atmospheric mercury at the Cape Hedo atmosphere and aerosol monitoring station (CHAAMS), Japan. *Environmental Science: Processes & Impacts*, *21*(5), 809–818. https://doi.org/10.1039/C8EM00590G